RSC Advances

PAPER

View Article Online
View Journal | View Issue

Cite this: *RSC Adv.*, 2016, **6**, 51485

Preparation and enhanced conducting properties of open networks of poly(3-hexylthiophene)/carbon nanotube hybrids

Gianfranco Sfuncia, Nunzio Tuccitto* and Giovanni Marletta

Received 13th April 2016
Accepted 13th May 2016

DOI: 10.1039/c6ra09592e

www.rsc.org/advances

The preparation of new high conductivity nanohybrid open networks of poly(3-hexylthiophene) and single-walled carbon nanotubes (P3HT/SWNTs) by spin coating deposition is reported. The novel open 2D-networks prepared at high spinning speed showed a conductivity three orders of magnitude higher than that measured for networks deposited at low spinning speed although the individual nanotubes are not seen to form a direct connection between the electrodes. The strong improvement of the conductivity performances is explained in terms of the formation of a new nanohybrid system consisting of thin sheaths of P3HT wrapped around SWNTs forming complex SWNT/P3HT/SWNT junctions yielding a soldering effect of the interposed P3HT sheath. The results open the way to molecular electronics devices exploiting the long-range conduction capability of nanotubes together with the thin P3HT sheath short range soldering effect at the hybrid nanowire junctions.

Introduction

Conjugated polymeric composites with carbon nanotubes are well known to provide a good conductive path at relatively low carbon content as these have high aspect ratio specific surfaces and are cost effective.[1] Many applications have indeed been proposed for conjugated polymer/carbon nanotube hybrid materials including conductive and high-strength composites, energy storage and energy conversion devices, sensors *etc.*[2,3] In particular, poly(3-hexylthiophene)/carbon nanotube composites (P3HT/NTs) are at the forefront of being widely used in the development of organic photovoltaic devices, chemical sensors *etc.*[4–8] Among the P3HT/NTs composites, those based on single-walled carbon nanotubes (P3HT/SWNTs) deserve particular interest in view of their optimal conductivity and efficiency performances in the framework of molecular electronics.[9–13]

The deposition/formation of a P3HT/SWNTs active layer on an appropriate device substrate is not an obvious process. In fact simple methods like P3HT solution casting produce almost amorphous films characterized by low charge carrier mobility due to the limited hopping process between disordered polymer domains while P3HT films prepared by spin coating may not yield the desired molecularly ordered nanowires because of fast solvent evaporation.[14] Nevertheless spin coating is still one of the most promising deposition techniques because of the uniformity of the deposited films the accurate control of the film thickness the low-temperature fabrication and the global high reproducibility of the technique. Furthermore the spin coated film structure may be adjusted by tuning the deposition conditions *i.e.* spin coated P3HT yields either macroscopic structures in the shape of long whiskers several micrometer long or nanocrystalline structure after spin coating and thermally annealing.[15,16] On the other hand spin coating deposition of active NTs layers is particularly tricky because of the need of appropriate surfactants or solvation conditions to achieve the dispersion of NTs.[17]

Accordingly to the above we have developed a dedicated strategy to prepare highly conductive P3HT/SWNTs nanocomposite layers by spin coating exploiting the strong affinity between P3HT chains with SWNTs and their wrapping capability to transfer hybrid nanowires P3HT/SWNTs in volatile organic solvents solution suitable for spin-coating process.[18–22] Such new hybrid system is shown to be formed by a thin sheath of P3HT wrapped around SWNTs allowing to conjugate the long range conduction capability of nanotubes with the short range "soldering effect" of P3HT sheath at the nanowire junctions between crossing P3HT/SWNTs.[23]

Experimental

Chemicals and preparation methods

Electronic grade regioregular poly(3-hexylthiophene-2,5-diyl) (P3HT) with Mn ranging between 54 000–75 000 g mol^{-1} and $M_w/Mn \leq 2.5$ single-wall carbon nanotubes (SWNTs) enriched in semiconductive species (SG76) with diameters comprised between 0.7–1.1 nm were obtained from Sigma-Aldrich (Milan Italy) and used without further purification.

Laboratory for Molecular Surfaces and Nanotechnology (LAMSUN), Department of Chemical Sciences, University of Catania and CSGI, Nunzio Tuccitto v.le A. Doria no. 6, 95125, Catania, Italy. E-mail: n.tuccitto@unict.it; Fax: +39 0957385206; Tel: +39 0957385206

All solvents used were CHROMASOLV® grade (Sigma-Aldrich). Ultrapure water (ρ = 18.2 MΩ cm) was obtained through a Milli-Q® purification system (Merck-Millipore). SWNTs–P3HT nanohybrids were obtained modifying a pre-existing protocol.[13] Few milligrams of P3HT were dissolved in 1,2-dichlorobenzene (DCB) to obtain a 0.5 mg mL^{-1} solution. Polymer chains disentanglement was promoted by a gentle warming the solution. A small quantity of SWNTs was dispersed in the P3HT/DCB solution so that the SWNTs/P3HT weight ratio was 1/3. To ensure nanotubes debundling the SWNTs/P3HT/DCB dispersion was tip-sonicated for 30 min keeping the vial in an ice bath to minimize solvent evaporation. The tip-sonicator (UP1000H Hielscher Germany) was used at the minimum of its power with a pulsed frequency of 0.5 s. As bundles are broken free nanotubes have the possibility to interact with P3HT polymer chains. Attractive interactions between them are strong and lead to the formation of stable supramolecular nanohybrid complexes in which the layer of adsorbed polymer chains hinders nanotubes intrinsic tendency to reaggregate as sonication ceases. During tip-sonication the dispersion display chromatic variations from orange to violet due to sonication-induced polymer crystallization. After sonication a small volume of the SWNTs/P3HT/DCB dispersion was diluted in toluene (ratio 1/10 total volume 1.5 mL) and centrifuged for 30 min at 10.000 g. The obtained nanohybrids-rich residue was then redispersed in 1.5 mL of chloroform briefly tip-sonicated and centrifuged for 1 hour at 10.000 g. Supernatant was hence collected and centrifuged again for 1 hour at 10.000 g. The nanohybrid-rich supernatant finally obtained was used for film deposition.

Substrates preparation and films deposition

Silicon ⟨100⟩ substrates purchased from Siegert (Cadolzburg Germany) were shortly bath-sonicated in different solvents of increasing polarity (chloroform > ethanol > water) and dry with nitrogen flux. Gold interdigitated electrodes (IDEs) consisting of an array of 180 pairs of microelectrodes ("fingers") on a pyrex substrate were purchased from MicruX Fluidic (Oviedo Spain). The active area of the array has a diameter of 3.5 mm. The fingers have widths and gaps of 5 μm and thickness of 120 nm measured by atomic force microscopy. IDEs are fabricated with a protective SU-8 layer which has to be removed prior their use. Ten cycles of cyclic voltammetry between −1.5 V and +1.5 V using H_2SO_4 0.1 N as electrolyte were executed to electrochemically etch this layer. IDEs were thereafter shortly bath-sonicated in water and isopropyl alcohol and dry with nitrogen flux. Spin-coating was chosen as deposition technique because of its large uniform coverage and reproducibility. Nanohybrids dispersion were deposited as thin films on silicon substrates for atomic force microscopy (AFM) characterization and on gold IDEs for electrical characterization. Spin-coating on silicon substrates was performed using 50 μL of the nanohybrids dispersion at angular velocities ranging from 100 to 3000 rpm. Spin-coating on gold IDEs was performed using 10 μL of the nanohybrids dispersion at angular velocities ranging from 100 to 3000 rpm.

Atomic force microscopy characterization

Nanohybrid films on silicon substrates and on gold IDEs were characterized by tapping-mode atomic force microscopy (AFM) using a Veeco Multimode with Nanoscope IIIa controller equipped with Tap300-G silicon probes (BudgetSensors) having force constant of 40 N m^{-1} and tip radius <10 nm. Section analysis were performed through a script (in Python™) to extract the trace of each scan and perform a statistical characterization (bearing analysis) of the whole scans.

Electrical characterization

Current-voltage characteristics of nanohybrid films on gold IDEs were recorded using a Keithley 2611-B Source-Measure Unit. *I–V* curves were recorded by applying voltage between −500 mV and +500 mV at 10 mV s^{-1} with a current sensitivity range of 10^{-8} Amp.

Results and discussion

Following the protocol detailed in the experimental section P3HT were dissolved and a small quantity of SWNTs was dispersed in the P3HT solution and sonicated to ensure nanotubes unbundling. As bundles are broken free nanotubes have the possibility to interact with P3HT polymer chains and lead to the formation of stable supramolecular hybrid assembly in which the layer of adsorbed polymer chains hinders nanotubes intrinsic tendency to reaggregate as sonication ceases. After sonication only the heavier bundle of nanotubes sediment while isolated nanohybrids remain well dispersed in the supernatant. The finally obtained nanohybrid-rich supernatant was used for film deposition. Several films spin-coated onto interdigitate electrodes (IDE) from the nanohybrid dispersion were prepared at varying speeds ranging from 100 to 3000 rpm resulted in different P3HT/SWNTs hybrids films. In Fig. 1 we report the wide scan AFM phase image of the structures formed onto interdigitated electrodes (IDE) by spin coating at 2000 rpm a dispersion of P3HT/SWNTs.

The phase image shows the deposition of a well-connected network of nanowires across and above the interdigitated electrodes. The nanowire height typically ranges from few to tens nm as shown in Fig. 2a which reports the high-resolution AFM height images. In this case the height is found (see section analysis in Fig. 2b) roughly constant both on top of the gold electrode and inside the gap.

Fig. 3 reports the different *I–V* characteristics of the networks as a function of the deposition spin speed. All samples show within the range of applied bias an ohmic behavior of the nanowire-based networks without significant asymmetry between the two polarities. Counterintuitively the networks obtained at slower deposition rate (100, 500 and 750 rpm) exhibit conduction performances that are up to 2 orders of magnitude lower than the networks deposited at higher deposition rates (1000, 2000 and 3000 rpm). Broadly speaking we can identify two basic conduction regimes: (1) networks deposited at speeds <1000 rpm showing low-conductivity; (2) networks deposited at speeds >1000 rpm exhibiting grouped higher

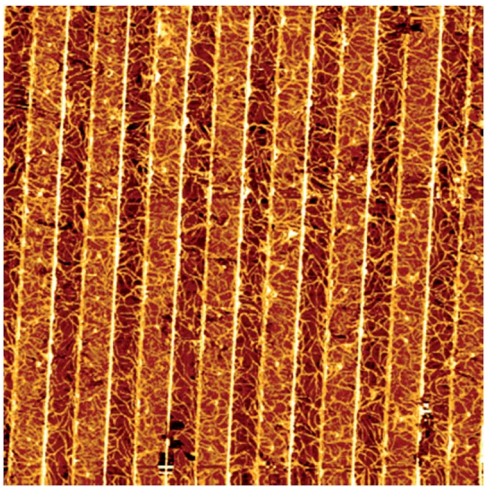

Fig. 1 Wide scan AFM phase false color image (field of scan 75 × 75 μm) of the structures formed by P3HT/SWNTs solution spin-coated at 2000 rpm onto 5 μm-wide interdigitated electrodes (IDE) with 5 μm gaps between them.

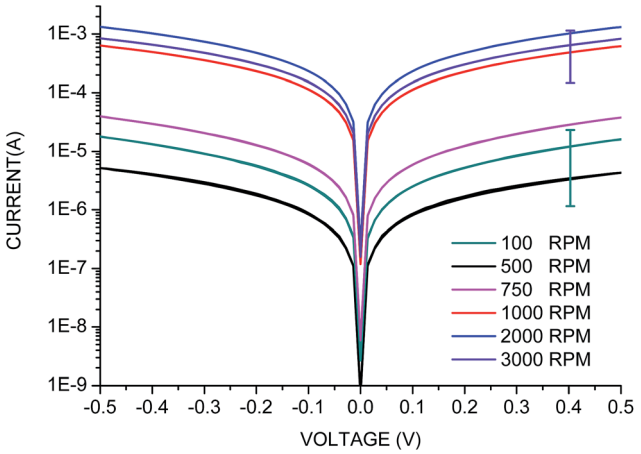

Fig. 3 *I–V* characteristic of samples prepared at various spin coating speeds (legend reports the respective rpm).

conductivity. To fully understand this behaviour a detailed study has been performed on the morphology at the nanoscale of the networks prepared on atomically flat silicon substrates. The results are very similar to those described for the IDE substrates: in particular, it has been found that the network density undergoes a marked decrease by increasing the spin speed. Adopting the substrate coverage as a marker of the network density we have found that at low spin speed (*i.e.* below 1000 rpm) the coverage ranges between 80 and 90% whilst at high spin speed (higher than 1000 rpm) the coverage is typically ranging from about 5 and 15%. Simultaneously also the thickness of the network structure decreases as the deposition speed is increased going from tens to a few nanometers suggesting the transition from dense 3D-to more open 2D-networks even if some overlapping between nanohybrids can be found in the latter case.

Fig. 4 reports the AFM height images and the related section analysis of two networks P3HT/SWNTs deposited on silicon substrates respectively assumed as archetypal of the two high and low density networks namely the ones respectively obtained at low (500 rpm Fig. 4a) and high speed (2000 rpm Fig. 4b).

Fig. 5 reports the heights distribution for both samples obtained through a statistical analysis performed on the AFM data. In the first case, a thick 3D-network the feature height distribution is large less than 100 nm and centered roughly

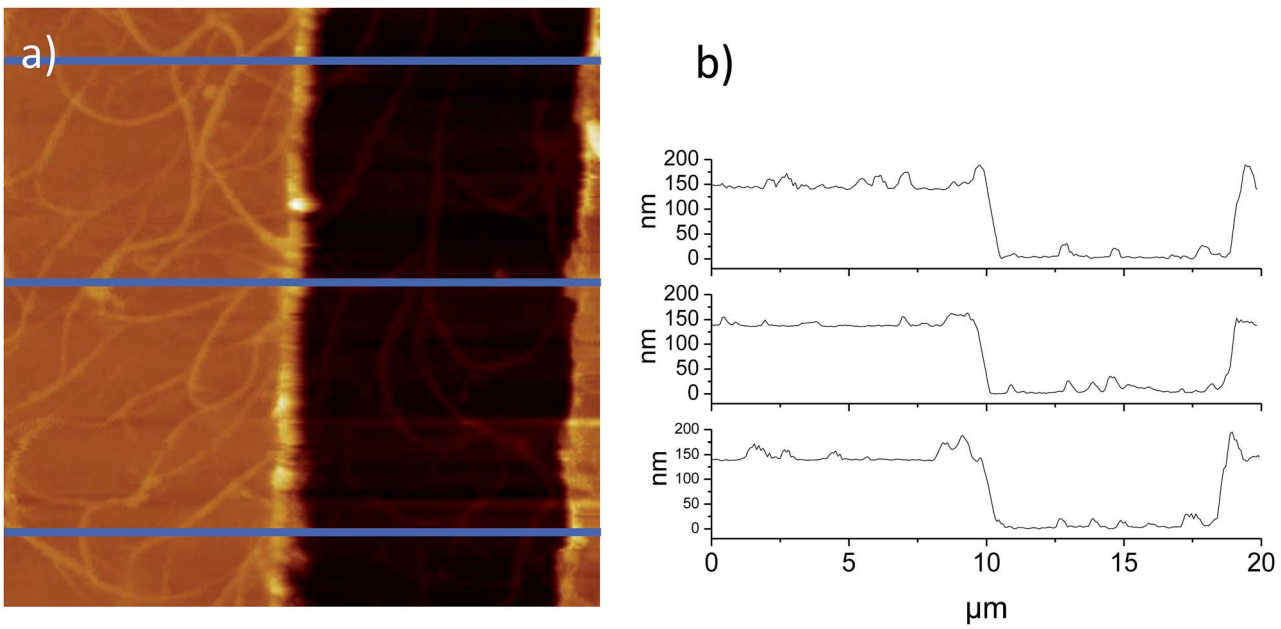

Fig. 2 (a) AFM height image (filed of scan = 20 × 20 μm *Z* scale = 500 nm) of the P3HT/SWNTs nanohybrids network deposited at 2000 rpm. (b) Height profiles acquired at the scans tracked in (a).

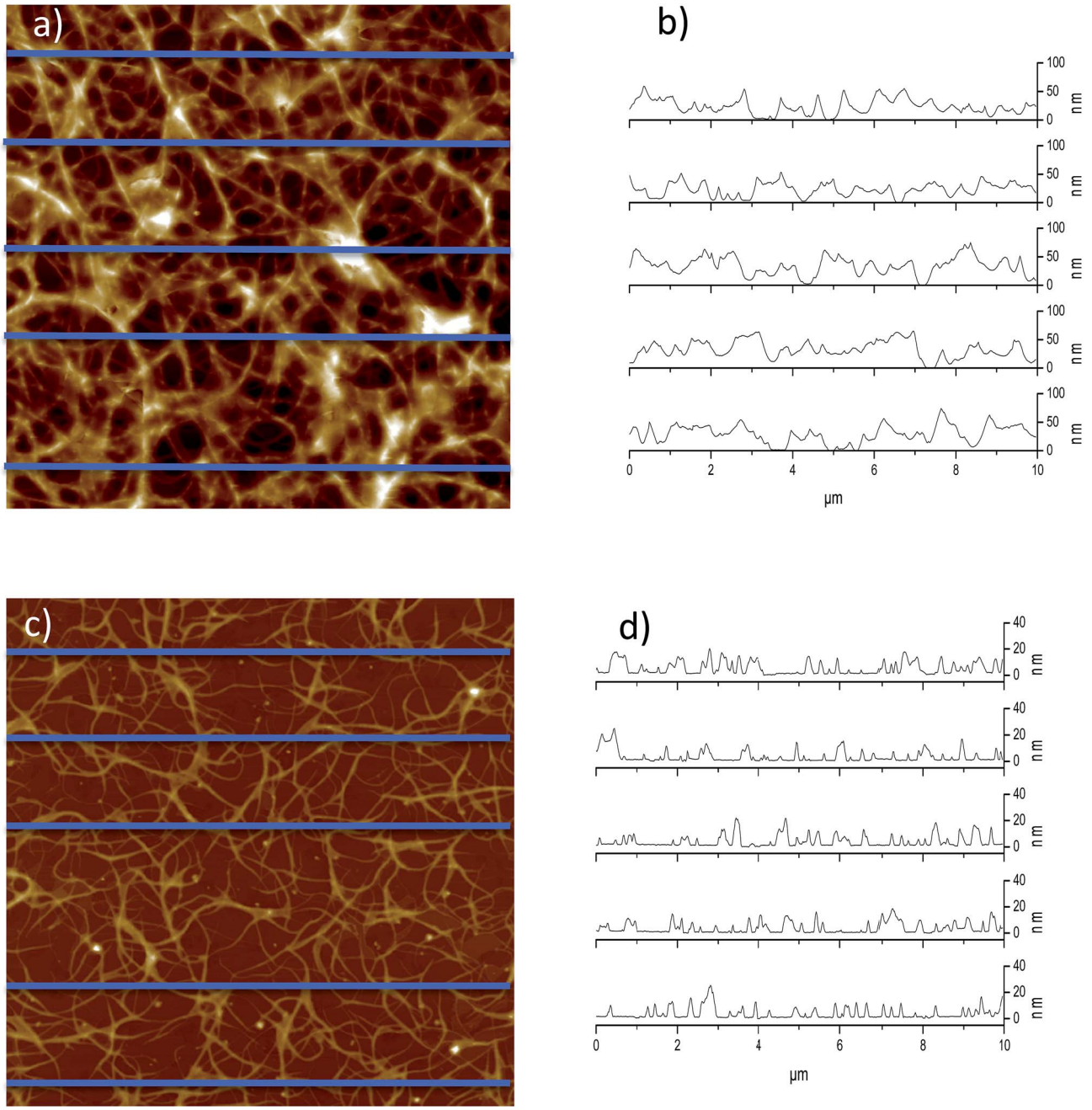

Fig. 4 (a) 10 × 10 μm AFM height image of the P3HT–SWNTs nanohybrids network deposited at 500 rpm on silicon (*Z* scale is 100 nm). (b) AFM height profiles acquired at the scans tracked in (a). (c) AFM height image of the P3HT–SWNTs nanohybrids network deposited at 2000 rpm on silicon (*Z* scale is 100 nm). (d) AFM height profiles acquired at the scans tracked in (c).

around 40 nm. This 3D-network contains a high number of overlapping junctions between the P3HT/SWNTs nanowires. On the contrary, the faster deposition rate produces a less dense 2D-network of P3HT/SWNTs meshes having narrow heights centred around 10 nm.

Fig. 4a and 5a suggest that the 3D-networks is basically formed by several layers of nanowires formed by single nanotubes or even bundles of them covered by a large amount of wrapping unstructured polymer (Fig. 4a). On the other hand, Fig. 4b and 5b suggest that the low-density 2D-network is consistent with a monolayer of nanowires, which are formed by a very thin P3HT layer wrapped around a single nanotube.

A confirmation of such hypothesis for high-speed deposited 2D networks can be figured out from the ultrahigh resolution height and phases AFM images reported in Fig. 6. The comparison between height and phase images reveals that the P3HT sheath is wrapped around each single nanotube forming a ribbon-like structure with an average 1 : 8 height/width aspect ratio. Indeed the section analysis of the phase signal (Fig. 6b and d) clearly shows the presence of the nanotubes inside the

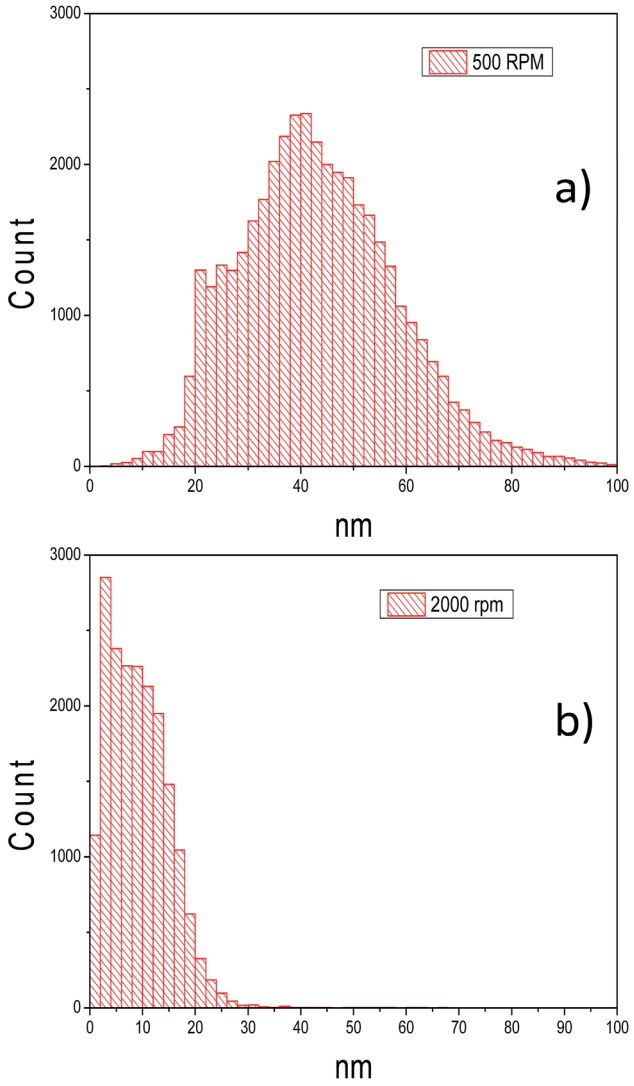

Fig. 5 (a) Statistical analysis of the structure heights reported in Fig. 4a. (b) Statistical analysis of the structure heights reported in Fig. 4c.

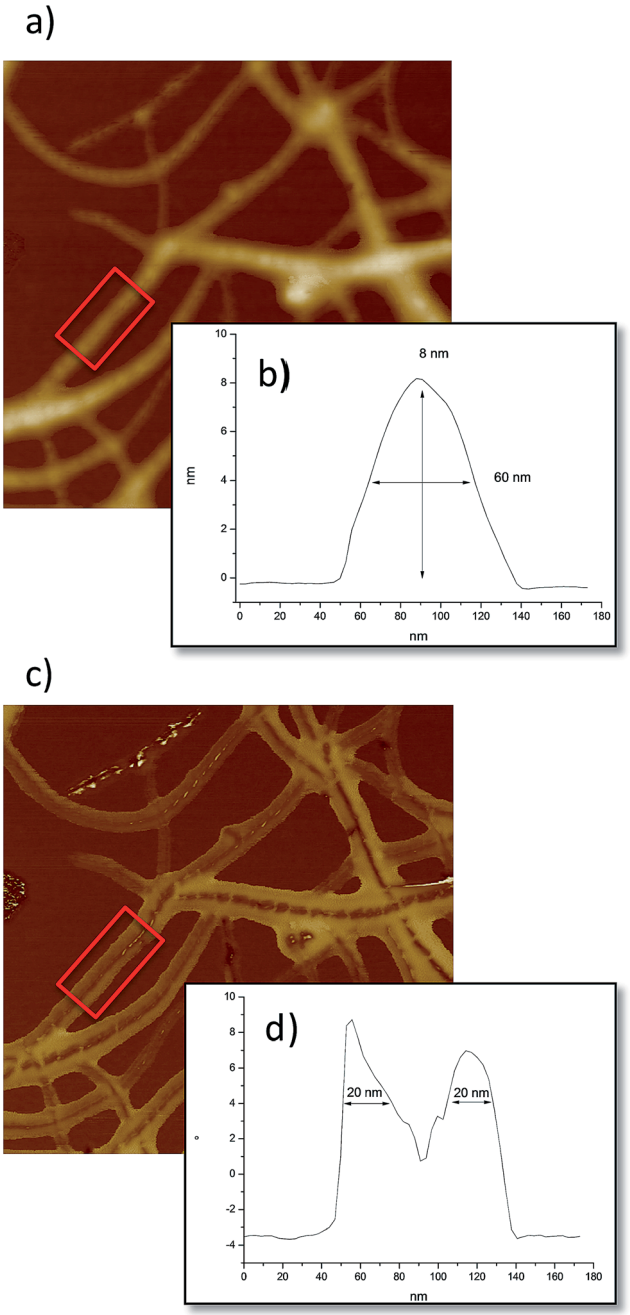

Fig. 6 a) 1.5 × 1.5 μm AFM height image of the P3HT–SWNTs nanohybrids network deposited at 2000 rpm on silicon (*Z* scale is 50 nm). (b) Averaged AFM height profile relative to the red box in (a). (c) 1.5 × 1.5 μm AFM phase image of the P3HT–SWNTs nanohybrids network deposited at 2000 rpm on silicon. (d) Averaged AFM phase profile relative to the red box in (c).

embedding cylindrical sheath of P3HT. The phase contrast between SWNTs and P3HT can be explained considering that nanotubes are much stiffer than soft polymers and that AFM phase signal is sensitive to variations of properties like viscoelasticity adhesion and friction.[24]

Notably the phase image allows also visualizing the inner structure of junctions formed by intercrossing nanohybrids. We estimate that the thickness of the P3HT layer around the tubes ranges from few to tens of nanometers forming therefore a nanohybrid material.

This picture suggests that at the highest deposition speed only the layers of P3HT that are intimately wrapped with SWNTs remains in the nanometric 2D network the high spinning velocity "peeling away" the excess of polymer.

Morphological characterization provided the whole networks thickness and an estimated coverage which can be used to estimate the bulk electrical conductivity (σ) roughly approximating the networks as simple thin films:

$$\sigma = LI/Wd\theta V$$

Accordingly σ is proportional to the measured current I under an applied voltage V, L, and W being respectively the spacing and the width of the electrodes. Two phenomenological parameters describe the P3HT/SWNTs networks in terms of

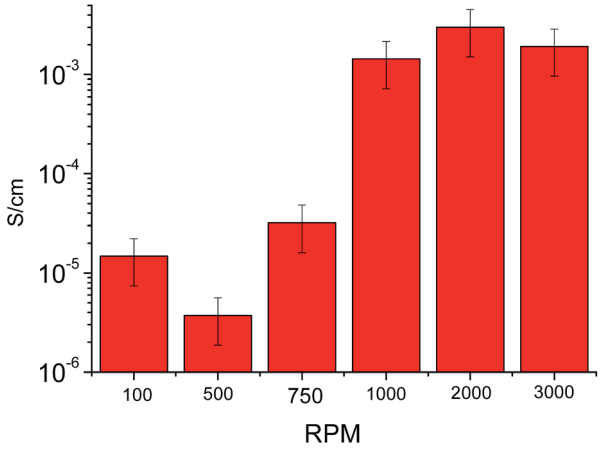

Fig. 7 Conductivity of P3HT/SWNTs nanohybrids as a function of the deposition speed (expressed in rpm).

ideal thickness (d) corresponding to the one of the meshes and effective area (θ) defined from the relative surface coverage.

The results reported in Fig. 7 confirm indeed the occurrence of two strongly different conductivity regimes respectively corresponding at low deposition speed to conductivity in the range of 10^{-6} to 10^{-5} S cm^{-1} and at deposition speed higher than 1000 rpm to a suddenly rising up conductivity 2–3 orders of magnitude higher. Most of the current studies deal with thick insulating polymer/NTs 3D-composites implying a conduction process essentially based on the percolation mechanism among NTs. Also for these systems the conductivity has been described in terms of two regimes depending on the NTs concentration respectively involving a lower conduction regime with low load of nanotubes and a second one working for highly concentrated samples where the nanotubes interact each other closely and the conductivity performances increase.[25] The conduction regimes in our samples work in the opposite way as far as the decrease of the loaded nanotubes significantly increases the

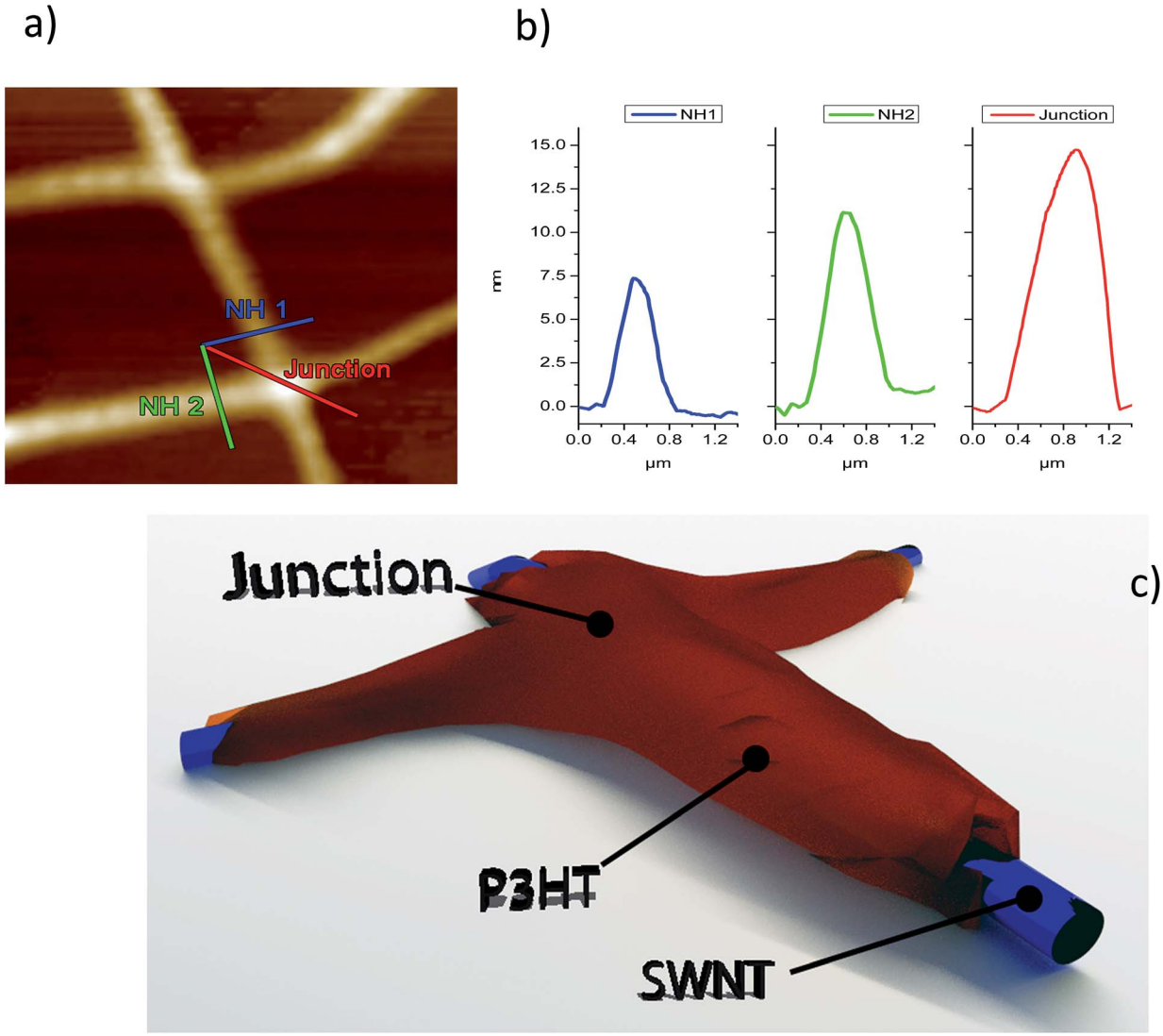

Fig. 8 (a) 750 × 750 nm AFM height image of P3HT/SWNTs nanohybrids deposited at 2000 rpm on silicon (digital zoom Z scale is 25 nm). (b) Height profiles relative to three traces in (b). (c) Schematic representation of a junction between two nanohybrids.

conduction performances. In particular the conductivity in our nanohybrid systems cannot occur by the inter-nanotube connections as in conventional thick composites because in our case the NTs are wrapped by a nanometric-thick continuous sheath of P3HT. This fact excludes the occurrence of a direct contact between crossing NTs whose junction resistance is known to constitute the highest contribution to resistance in the percolating electrical pathways substantially concurring to the total resistivity of these films.[23]

Therefore we propose that the unusual conductivity performances of the 3D and 2D nanohybrid networks are due to the effect of the P3HT sheath around the NTs. Indeed according to recent literature,[26] for nanohybrid structures of isolated SWNT coated with a monolayer of P3HT in solution it has been shown by means of ultrafast spectroscopy measurements that the intimate contact between the P3HT sheath and the nanotube yields the enhancement of the charge transfer process between the two materials. In particular the polymer sheath emission in the P3HT–SWNT samples exhibits an ultrafast decay prompting the charge separation efficiency at variance of the long-lived decay and lower charge separation observed for bulk P3HT.

The nanohybrids described in the present letter are however different from the isolated P3HT–SWNT hybrid structures in solution as far as the nanowires deposited on solid substrates in our case yield a large number of crossing points in the 3D or 2D networks where complex SWNT/P3HT/SWNTs junctions are formed. In particular in the 2D networks the wrapping sheaths around SWNT and the related junctions are thinner than those measured in the 3D networks.

Fig. 8 reports the AFM height images of two nanohybrids junctions in the thinner 2D confirming the presence of a very thin layer of P3HT between two overlapping tubes in correspondence of the junction. Furthermore it is noteworthy (Fig. 8b) that the height of the three term junctions is lower than the sum of isolated nanohybrids wires suggesting that these are not just overlapping keeping the sheath structure of the isolated wires but are modified in a peculiar way in the sandwiching regions.

In this framework the thinner sheaths of P3HT are thought to act as a better electrical connecting medium at the hybrid nanowire junctions. In fact the polymer sheath at these junctions under charge injection would play an active role in the charge transport between the wrapped NTs producing a similar improvement of the electrical performances as in the case of carbon nanotube networks functionalized by *in situ* polymerization of a thin layer of conducting polymer[27] or by nanosoldering of junctions with metallic nanoparticles.[23] In fact according to the electrical measurements reported above (Fig. 2) we correlate the three orders of magnitude improvement in the conductivity measured for 2D networks to the P3HT sheath thinning produced at higher spin speeds in the junction regions in the 2D networks. Furthermore the correlation between electrical and morphological data for the various networks indicates the existence of a threshold in the thickness of the P3HT sheath in order to observe the conductivity enhancement. In the present experimental conditions this threshold is of the order of 20 nm *i.e.* the value measured for the most efficient conducting 2D networks.

Conclusions

In summary we have described new hybrid P3HT/SWNT networks consisting in a tuneable thickness thin sheath of P3HT wrapping SWNTs yielding the increase up to three orders of magnitude of conductivity depending on the thickness of the P3HT sheath structure around SWNTs. This result open the way to new highly conducting polymer-based devices efficiently joining the long range conduction capability of SWNTs and the polymer-based junction soldering effect of P3HT sheath between two SWNTs working on distances of several microns.

Acknowledgements

The authors gratefully acknowledge the financial support of PON02_00355_3391233 – ENERGETIC (MIUR Italy).

Notes and references

1 W. Bauhofer and J. Z. Kovacs, *CNT-NET 07 Special Issue with regular papers*, 2009, vol. 69(10), pp. 1486–1498.
2 R. Baughman, A. Zakhidov and W. de Heer, *Science*, 2002, **297**(5582), 787–792.
3 B. Dinesh, M. Squillaci, C. Menard-Moyon, P. Samori and A. Bianco, *Nanoscale*, 2015, **7**(38), 15873–15879.
4 R. Hatton, N. Blanchard, L. Tan, G. Latini, F. Cacialli and S. Silva, *Org. Electron.*, 2009, **10**(3), 388–395.
5 M. Cai, V. Tiong, T. Hreid, J. Bell and H. Wang, *J. Mater. Chem. A*, 2015, **3**(6), 2784–2793.
6 N. Mzoughi, A. Abdellah, Q. Gong, H. Grothe, P. Lugli, B. Wolf and G. Scarpa, *Sens. Actuators, B*, 2012, **171**, 537–543.
7 S. Yang, D. Meng, J. Sun, Y. Huang and J. Geng, *ACS Appl. Mater. Interfaces*, 2014, **6**(10), 7686–7694.
8 W. Hou, N.-J. Zhao, D. Meng, J. Tang, Y. Zeng, Y. Wu, Y. Weng, C. Cheng, X. Xu, Y. Li, J.-P. Zhang, Y. Huang, C. W. Bielawski and J. Geng, *ACS Nano*, 2016, DOI: 10.1021/acsnano.6b00673.
9 J. Niklas, J. Holt, K. Mistry, G. Rumbles, J. Blackburn and O. Poluektov, *J. Phys. Chem. Lett.*, 2014, **5**(3), 601–606.
10 S. Ren, M. Bernardi, R. Lunt, V. Bulovic, J. Grossman and S. Gradecak, *Nano Lett.*, 2011, **11**(12), 5316–5321.
11 J. Holt, A. Ferguson, N. Kopidakis, B. Larsen, J. Bult, G. Rumbles and J. Blackburn, *Nano Lett.*, 2010, **10**(11), 4627–4633.
12 Y. Kanai and J. Grossman, *Nano Lett.*, 2008, **8**(3), 908–912.
13 T. Schuettfort, H. Snaith, A. Nish and R. Nicholas, *Nanotechnology*, 2010, **21**(2), 025201.
14 K. Aasmundtveit, E. Samuelsen, M. Guldstein, C. Steinsland, O. Flornes, C. Fagermo, T. Seeberg, L. Pettersson, O. Inganas, R. Feidenhans'l and S. Ferrer, *Macromolecules*, 2000, **33**(8), 3120–3127.
15 N. Seidler, G. Lazzerini, G. Li Destri, G. Marletta and F. Cacialli, *J. Mater. Chem. C*, 2013, **1**(46), 7748–7757.

16 G. Li Destri, T. Keller, M. Catellani, F. Punzo, K. Jandt and G. Marletta, *Macromol. Chem. Phys.*, 2011, **212**(9), 905–914.
17 J. Jo, J. Jung, J. Lee and W. Jo, *ACS Nano*, 2010, **4**(9), 5382–5388.
18 M. Giulianini, E. Waclawik, J. Bell, M. Scarselli, P. Castrucci, M. De Crescenzi and N. Motta, *Appl. Phys. Lett.*, 2009, **95**(14), 143116.
19 J. Geng and T. Zeng, *J. Am. Chem. Soc.*, 2006, **128**(51), 16827–16833.
20 M. Giulianini, E. Waclawik, J. Bell, M. De Crescenzi, P. Castrucci, M. Scarselli, M. Diociaiuti, S. Casciardi and N. Motta, *J. Phys. Chem. C*, 2011, **115**(14), 6324–6330.
21 M. Giulianini, E. Waclawik, J. Bell, M. Scarselli, P. Castrucci, M. De Crescenzi and N. Motta, *Polymers*, 2011, **3**(3), 1433–1446.
22 M. Bernardi, M. Giulianini and J. Grossman, *ACS Nano*, 2010, **4**(11), 6599–6606.
23 J. Do, D. Estrada, X. Xie, N. Chang, J. Mallek, G. Girolami, J. Rogers, E. Pop and J. Lyding, *Nano Lett.*, 2013, **13**(12), 5844–5850.
24 P. Eaton and P. West, *Atomic force microscopy*, Oxford University Press: Oxford, 2010, vol. viii, p. 248.
25 A. Musumeci, G. Silva, J. Liu, W. Martens and E. Waclawik, *Polymer*, 2007, **48**(6), 1667–1678.
26 S. Stranks, C. Weisspfennig, P. Parkinson, M. Johnston, L. Herz and R. Nicholas, *Nano Lett.*, 2011, **11**(1), 66–72.
27 Y. Ma, W. Cheung, D. Wei, A. Bogozi, P. Chiu, L. Wang, F. Pontoriero, R. Mendelsohn and H. He, *ACS Nano*, 2008, **2**(6), 1197–1204.